ACKNOWLEDGMENT

This work was supported by the U.S. Department of Energy Office of Inertial Fusion under agreement No. DE-FC08-85DP40200, and by the Laser Fusion Feasibility Project at the Laboratory for Laser Energetics, which has the following sponsors: Empire State Electric Energy Research Corporation, General Electric Company, New York State Energy Research and Development Authority, Ontario Hydro, and the University of Rochester. Such support does not imply endorsement of the content by any of the above parties.

REFERENCES

1. W.C. Mead *et al.*, *Phys. Rev. Lett.* **47**, 1289 (1981).
2. W. Seka, R. S. Craxton, J. Delettrez, L. Goldman, R. Keck, R. L. McCrory, D. Shvarts, J. M. Soures, and R. Boni, *Opt. Commun.* **40**, 437 (1982).
3. C. Garban-Labaune *et al.*, *Phys. Rev. Lett.* **48**, 1018 (1982).
4. D. C. Slater *et al.*, *Phys. Rev. Lett.* **46**, 1199 (1981).
5. M. C. Richardson, R. S. Craxton, J. Delettrez, R. L. Keck, R. L. McCrory, W. Seka, and J. M. Soures, *Phys. Rev. Lett.* **54**, 1656 (1985).

## 1.C A Source of Hot Spots in Frequency-Tripled Laser Light

To achieve the high-density compressions required for thermonuclear ignition with direct-drive laser fusion, very smooth laser intensity profiles must be obtained in the target plane. Intensity variations around a smooth envelope must be less than about $\pm 10\%$. The effect of beam structure would be to implode some portions of the target faster than others and to "seed" the Rayleigh-Taylor hydrodynamic instability, resulting in reduced spherical convergence of the target, mixing between the shell and fuel, and a substantially degraded neutron yield. Considerable effort has been expended at LLE to determine the present quality of the OMEGA laser beams, and to determine what improvements might be necessary to meet the high-density milestones set for the OMEGA system. An important achievement of this uniformity program is that for the first time there is an understanding of what causes the observed laser-beam intensity variations in the target plane.

Detailed examination of the equivalent-target-plane (ETP) image of an OMEGA UV test beam has shown the presence of numerous hot spots with peak-to-valley variations of about 2 to 1 and spot widths of about 5% to 10% of the target diameter. The hot spots were found to occur only in focused, frequency-tripled UV light; they were relatively insignificant in the fundamental IR beam, which was dominated by long-wavelength structure (Fig. 31.11). The research effort to improve beam uniformity concentrated on identifying what aspect of the frequency-tripling process is responsible for the generation of the hot-spot structure. The answer was found by combining high-resolution

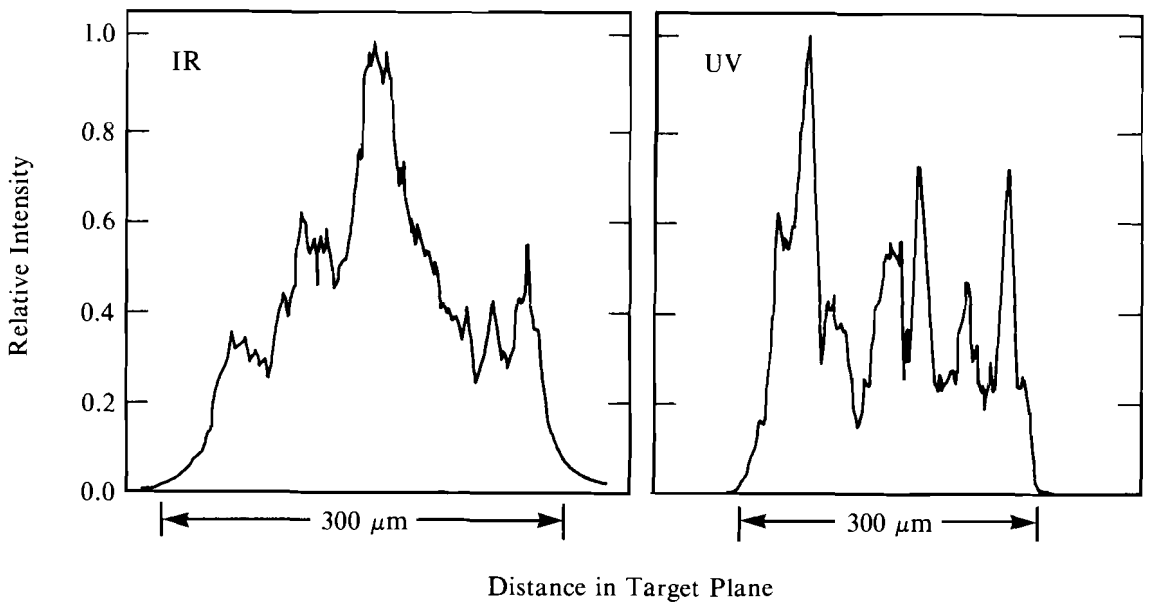


Fig. 31.11
Measured equivalent-target-plane (ETP) image for an IR beam and a frequency-tripled UV beam. Frequency tripling was observed to produce hot spots in the target-plane beam profile.

phase measurements of the near-field beam with computer modeling of the beam propagation to the target plane. The source of the hot spots lies in the phase error of the IR laser system, before conversion occurs.

Phase error is introduced by variations in the index of refraction $\Delta n$ across the beam. The resulting variation in optical path length $\Delta\ell$ of rays with geometric path length $\ell$ is $\Delta\ell = \Delta n\ell$; the phase error is $\phi = k\Delta\ell$, where $k$ is the wave number of the light. (Additional phase error can be introduced by variations in $\ell$ for different rays.) For a beam propagating in the $z$ direction, the electric field depends on the phase error as $E(\text{IR}) \sim \exp[ik_o(z+\Delta\ell)]$, where the subscript $o$ refers to IR light. The shape of the wave front is given by the term in parenthesis: $z+\Delta\ell$ = constant. During frequency conversion, the wave front is not changed; only the wave number is tripled—i.e., $E(\text{UV}) \sim \exp[i3k_o(zz+\Delta\ell)]$. A geometrical optics analysis would say that the UV and IR beams should show identical structure, since propagation is in the direction normal to the wave front, and they both have the same front. However, as the far field of the focusing lens is approached, diffractive effects will set in, and the two wavelengths of light will behave differently. If the phase error $\phi$ is sufficiently large, the beam will act as if it had been broken up into small beamlets, each with its own diffraction pattern; interference between the beamlets can lead to substantial hot spots. For the formation of beamlets to occur, the phase variation should be greater than about $2\pi/10$ rad and have a spatial variation smaller than about 1/10 the beam diameter. Since the phase error relative to the light wavelength is tripled upon frequency

conversion, IR phase errors as small as $2\pi/15 - 2\pi/30$ are enough to cause beamlet formation in the resulting UV-converted beam.

One of the 24 OMEGA beamlines was examined in detail to identify the sources of phase error. Phase errors can occur within the amplification chain, the frequency-conversion crystals, and the transport optics, as well as during beam propagation through the air to the target chamber. For high-efficiency frequency conversion, the UV light must have the same phase structure as the IR; the high optical quality of the conversion crystals in the test beam precluded the introduction of any additional, significant phase error during the frequency-tripling process. Also, no significant amplitude errors are introduced during conversion, as the measured near-field UV images show a relatively smooth profile (Fig. 31.12). Atmospheric turbulence was found to be one source of phase error that produced varying amounts of hot-spot structure. By enclosing part of the test beam in a corridor, thus isolating it from air fluctuations within the laser bay, some reduction in the hot-spot amplitude was observed, together with increased shot-to-shot reproducibility of the beam structure—though a major portion of the hot-spot structure still remained. Thus, for this beamline the damaging phase error must be inherent in the IR laser chain. These errors can be passive, due to imperfections in the amplifying medium and optical elements, or dynamic, due to variations in the index of refraction of amplifier glass arising from, for instance, thermal stress from flashlamp radiation. A high-resolution measurement of the IR near-field phase was made (as discussed in the article entitled "High-Power Laser Interferometry" appearing in this issue) to search for the small-scale structure that might lead to target-plane hot spots.

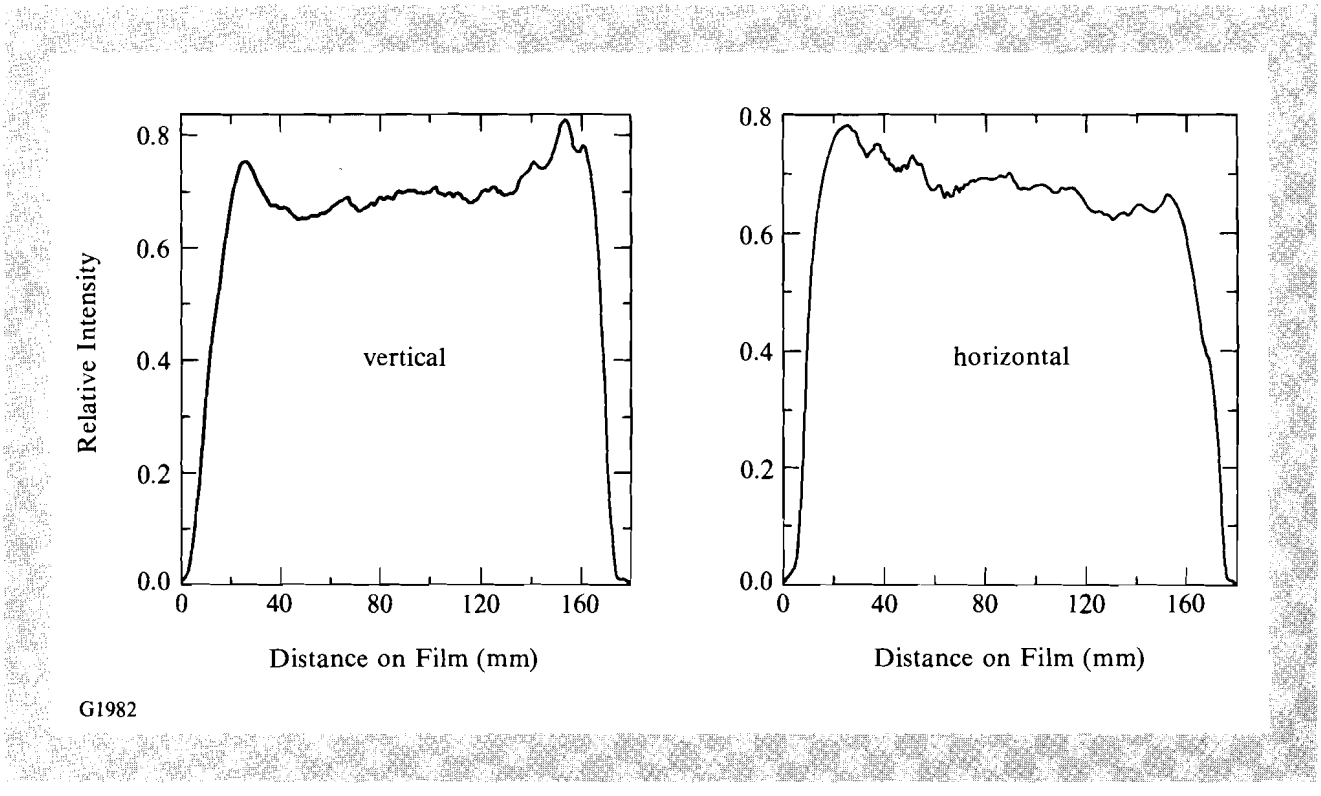


Fig. 31.12
Measured near-field UV image. No large amplitude variations were observed in the near field.

The effect of the near-field phase errors on the target-plane beam profile was determined by computer simulation of the beam propagation. The numerical model treated the laser propagation according to scalar diffraction theory using Kirchhoff-Huygens boundary conditions. Each component of the laser electric field at a point $\boldsymbol{r}$ is described by the scalar quantity $U(\boldsymbol{r})$ and is related to the near-field amplitude $A$ and phase according to[1]

$$U(\boldsymbol{r}) = -i\frac{F}{\lambda}e^{-ikF}\int e^{ik(d+\Delta\ell)}A\,d\Omega/d \quad , \tag{1}$$

where the integration is over the near-field aperture, $F$ is the lens focal length, and $d$ is the distance to the point $\boldsymbol{r}$ from a point $\boldsymbol{R}$ on the lens (Fig. 31.13). Following Born and Wolf, we make the following approximation:

$$d-F = \hat{\boldsymbol{q}} \cdot \boldsymbol{r}$$

appropriate near the focal plane ($r/F \ll 1$), but not necessarily in the far field. Equation (1) simplifies to

$$U(\boldsymbol{r}) = -\frac{i}{\lambda}\int e^{-ik(\hat{\boldsymbol{q}}\cdot\boldsymbol{r}-\Delta\ell)}A\,d\Omega \quad . \tag{2}$$

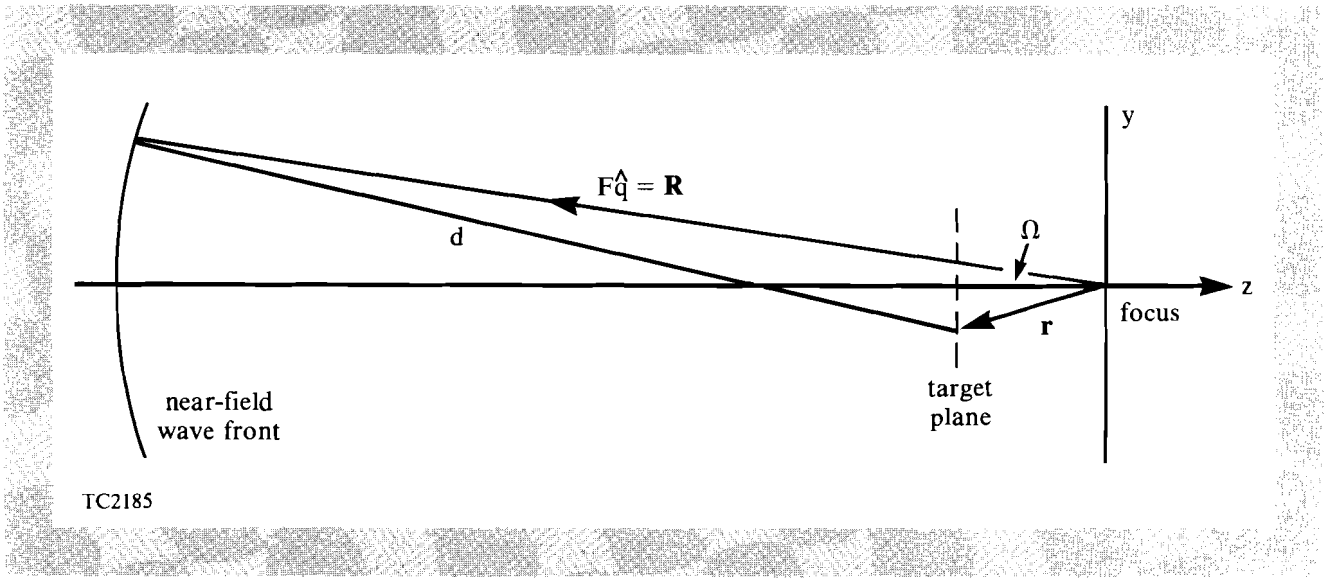


Fig. 31.13
Geometry and variables used in the beam propagation calculation.

The coordinates of $\boldsymbol{r}$ and $\boldsymbol{R}$ are defined to be $(x,y,z)$ and $(X,Y,Z)$, respectively. Since the point $\boldsymbol{R}$ lies on a spherical wave front of radius $F$, the value of $Z$ is $Z = -(F^2 - X^2 - Y^2)^{1/2}$, which is approximated by

$$Z = -F\left[1-\frac{1}{2}(X^2+Y^2)/F^2 \ldots\right] \quad . \tag{3}$$

Keeping the first two terms in brackets is the Fresnel approximation, which is appropriate for the quasi-near-field plane, where OMEGA targets are positioned.

Equation (2) was solved by dividing the near-field aperture into a 100 × 100 square computational grid. The amplitude $A$ and phase $\phi$ were assumed to be constant in each computational cell. Combining Eq. (3) with Eq. (2) yields

$$U(r) = -\frac{i}{\lambda}\sum_{i,j} A_{i,j}\, e^{-ik(\Delta\ell_{ij}-z)} \times \int_i e^{-ik(xX/F-\frac{1}{2}z\,X^2/F^2)}dX \times \int_j e^{-ik(yY/F-\frac{1}{2}zY^2/F^2)}dY \quad . \tag{4}$$

The $X$ and $Y$ integrations are across cell $ij$, from $X_i$ to $X_{i+1}$ and $Y_j$ to $Y_{j+1}$, respectively. The integrations were written in terms of the standard Fresnel integrals and were evaluated from numerical tables. The target-plane laser intensity is then proportional to $|U(r)|^2$.

The near-field amplitude and phase are inputs to the propagation code. The near-field amplitude profiles of Fig. 31.12 were typical of all shots, for both the IR and UV, having intensity modulations of $\pm 10\%$. Very little structure is observed; in fact, the amplitude could be replaced by a smooth supergaussian in the code with very little effect on the calculated TP image—i.e., phase error completely dominates the beam structure. An example of the measured phase error for two perpendicular cuts through the beam is shown in Fig. 31.14. The long-wavelength structure is responsible for shifting the position of the beam and distorting its general shape, as seen in the IR image in Fig. 31.11. The small-scale structure has relatively low modulation, but this is the source of the UV hot spots.

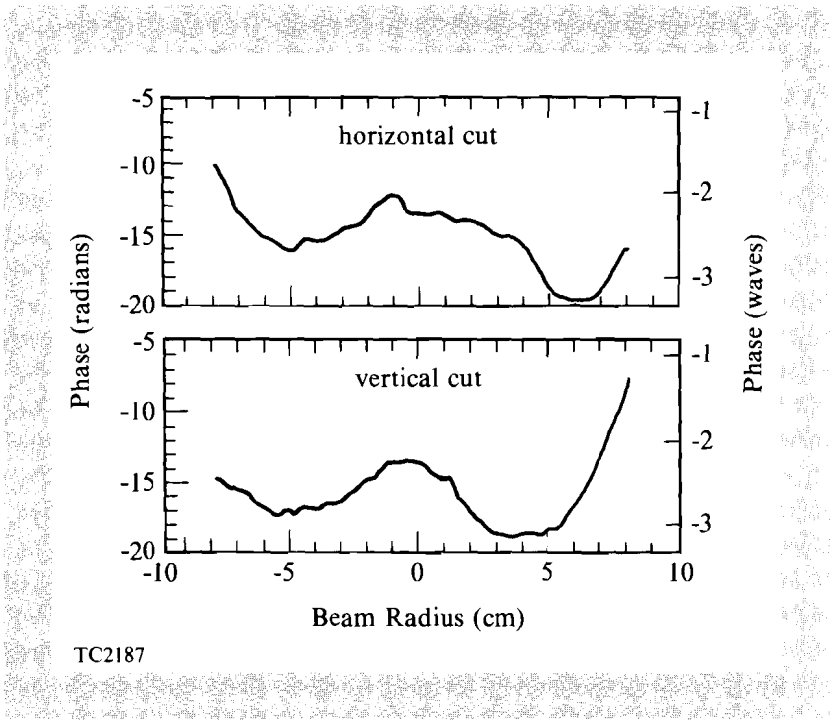


Fig. 31.14
Measured near-field phase error. Some small-scale structure is visible, and this leads to hot-spot formation. The phase was measured in the IR and has been multiplied here by 3 for the UV calculation.

A comparison between a calculated IR target-plane image and a measured ETP image is shown in Fig. 31.15. The characteristic features of the profile have been reproduced, specifically, the central peak and its width, and in the horizontal cut the shift of the central peak and the appearance of a peak on the edge. The last feature is the only structure predominantly caused by the near-field amplitude, which had one edge slightly more intense than the rest of the beam. A supergaussian near-field amplitude with the measured phase error reproduces all the structure except that one edge peak.

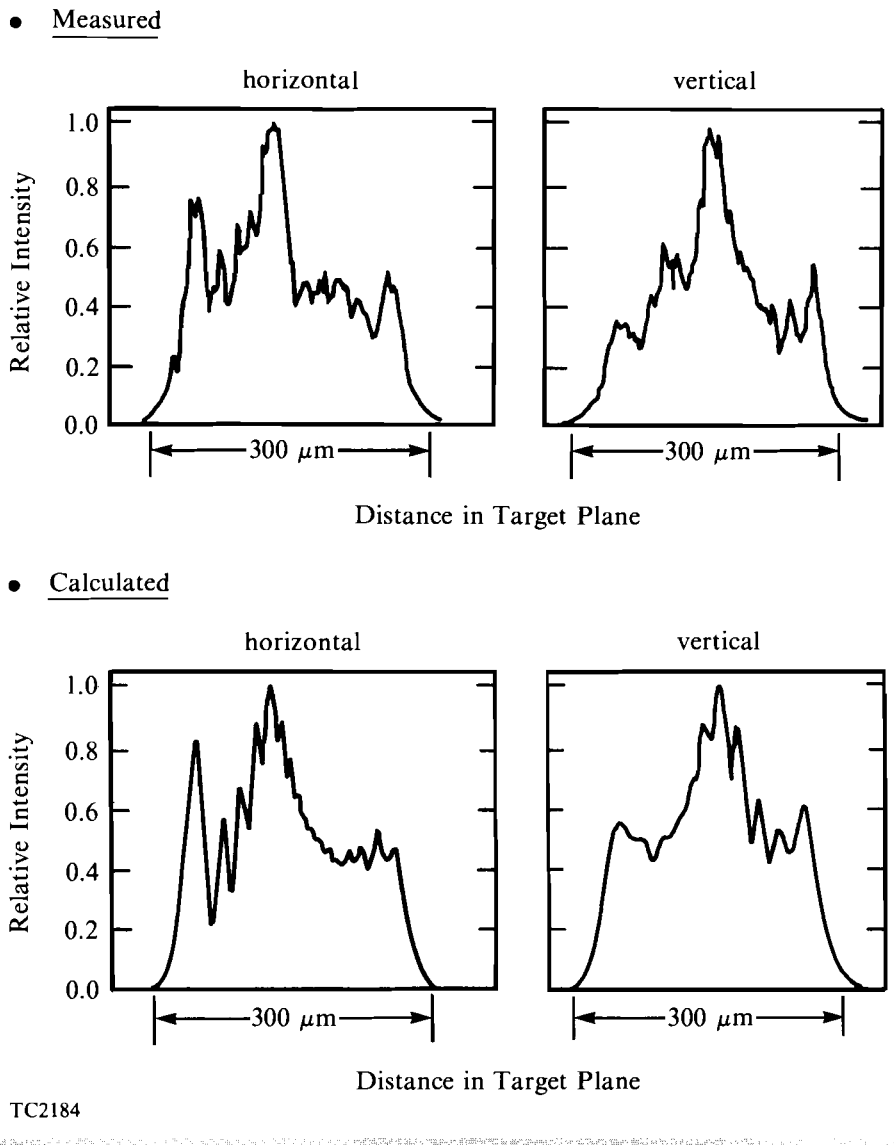


Fig. 31.15
Using measured near-field amplitude and phase variations, an IR target-plane profile was calculated. The general features of the measured ETP image have been reproduced.

The main question is whether the phase error can simultaneously account for the structure in both the IR and UV target-plane images. The result is shown in Fig. 31.16. A supergaussian near-field amplitude was used to demonstrate unequivocally that the hot-spot formation is primarily dominated by phase error. The same phase error was used in both the UV and IR calculations, the only difference in the calculations being the wavelength of the light. Comparing Figs. 31.11 and 31.16, we see that the observed beam breakup into hot spots, in going from the IR to the UV, has been well reproduced.

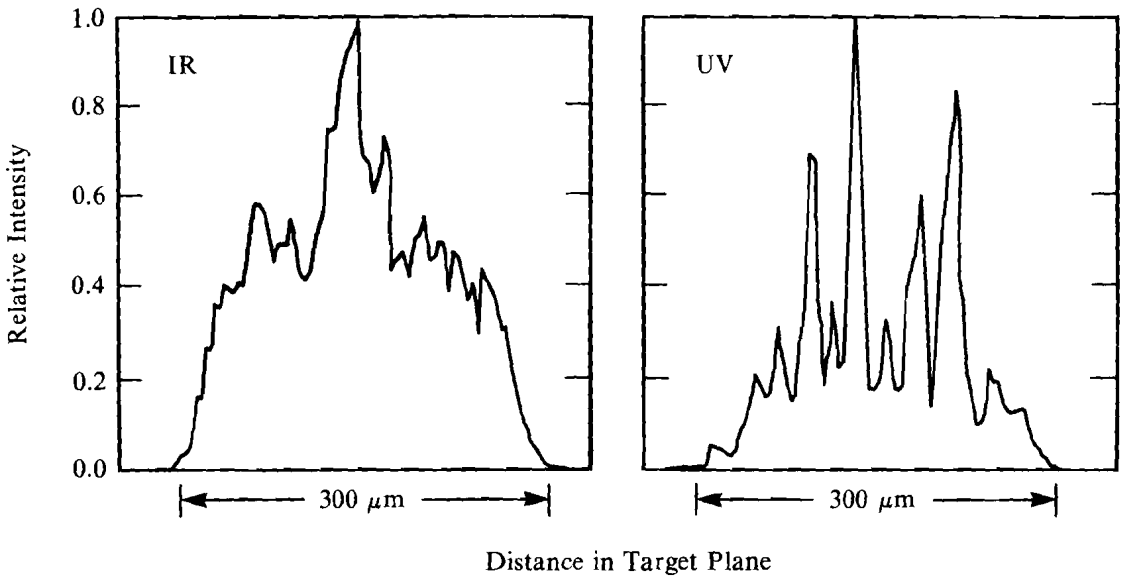


Fig. 31.16
Calculated target-plane images for an IR and a UV beam. Both calculations used the same near-field amplitude (supergaussian) and the same measured phase error (Fig. 31.14); only the light wavelength was different. The IR image is slightly different than the one shown in Fig. 31.15 because a different set of phases and amplitudes was used. Hot-spot structure is produced in the UV but not in the IR calculation, in agreement with the experimental observation (Fig. 31.11).

The breakup of the UV beam appears to be the result of small-scale-length phase errors. When the phase error exceeds about $2\pi/10$, the beam effectively breaks up into separate beamlets. Similar behavior was found computationally by imposing a 10 x 10 square random-phase mask on a beam with otherwise perfect phase. The phase of each cell in the mask was chosen randomly between 0 and $2\pi/3$. This configuration produced hot-spot structure similar to that seen in the UV target-plane image. When the phase error was reduced by a factor of 3 for the corresponding IR calculation, the hot-spot structure disappeared.

As a result of combining high-resolution phase measurements with computer modeling, the reason for the appearance of the hot-spot structure in the UV beam (and its absence in the IR) is now well understood. The code is now being used to investigate various strategies for improving beam uniformity, such as random-phase masks.

## ACKNOWLEDGMENT

This work was supported by the U.S. Department of Energy Office of Inertial Fusion under agreement No. DE-FC08-85DP40200, and by the Laser Fusion Feasibility Project at the Laboratory for Laser Energetics, which has the following sponsors: Empire State Electric Energy Research Corporation, General Electric Company, New York State Energy Research and Development Authority, Ontario Hydro, and the University of Rochester. Such support does not imply endorsement of the content by any of the above parties.

## REFERENCES

1. M. Born and E. Wolf, *Principles of Optics*, 6th ed. (Pergamon Press, Oxford, 1986), pp. 436–437.